Analyst

Accepted Manuscript

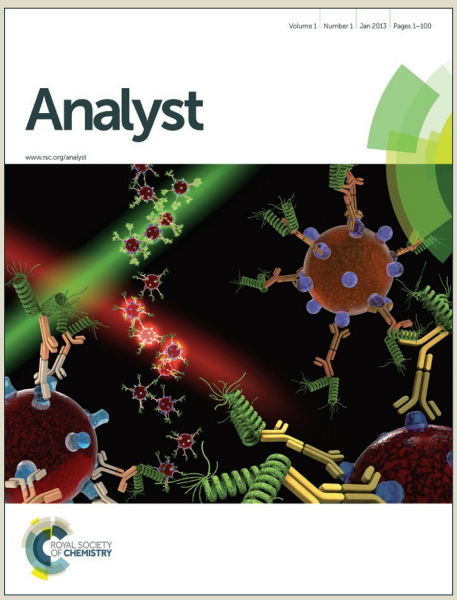

ROYAL SOCIETY OF CHEMISTRY

www.rsc.org/analyst

For *Analyst* as a Full paper:

Sample stage designed for force modulation microscopy using a tip-mounted AFM scanner

Lu Lu,[1] Song Xu,[2] Donghui Zhang[1] and Jayne C. Garno[1]*

[1]Department of Chemistry, Louisiana State University, 232 Choppin Hall, Baton Rouge, LA 70803 USA

[2]Keysight Technologies, 1400 Fountaingrove Parkway, Santa Rosa, CA 95403 USA

Corresponding author: Jayne C. Garno

Phone: 225-578-8942;

FAX: 225-578-3458;

E-mail: jgarno@lsu.edu

Abstract

Among the modes of scanning probe microscopy (SPM), force modulation microscopy (FMM) is often used to acquire mechanical properties of samples concurrent with topographic information. The FMM mode is useful for investigations with polymer and organic thin film samples. Qualitative evaluation of the mixed domains of co-polymers or composite films can often be accomplished with high resolution using FMM phase and amplitude images. We have designed and tested a sample stage for FMM constructed of machined polycarbonate. A generic design enables FMM experiments for instrument configurations with a tip-mounted SPM scanner. A piezoactuator within the sample stage was used to drive the sample to vibrate in the z-direction according to selected parameters. To evaluate the FMM sample stage, we tested samples of known composition with nanoscale dimensions for increasingly complex surface morphologies. Excellent resolution was achieved in ambient conditions using the home-constructed sample stage, as revealed for complex surfaces or multi-component samples. Test structures of nanoholes within a film of organosilanes provided the simplest platform with two distinct surface domains. Ring-shaped nanostructures prepared on Si(111) with mixed organosilanes provided three regions for evaluating FMM results. A complex sample consisting of a cyclic gel polymer containing fibril nanostructures was also tested with FMM measurements. Frequency spectra were acquired for sample domains, revealing distinct differences in local mechanical response. We demonstrate a practical approach to construct a sample stage accessory to facilitate z-sample modulation for FMM experiments with tip-mounted SPM scanners.

TOC graphic

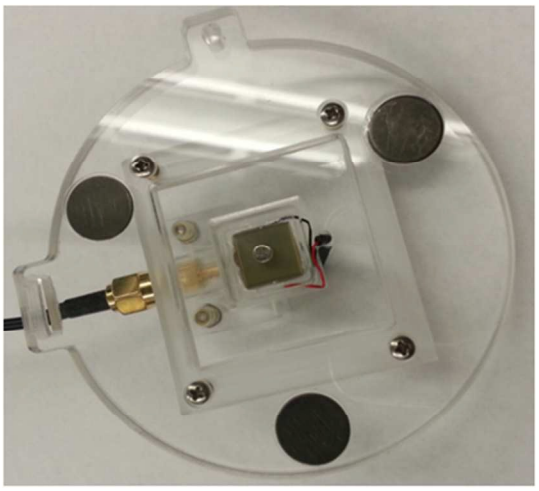

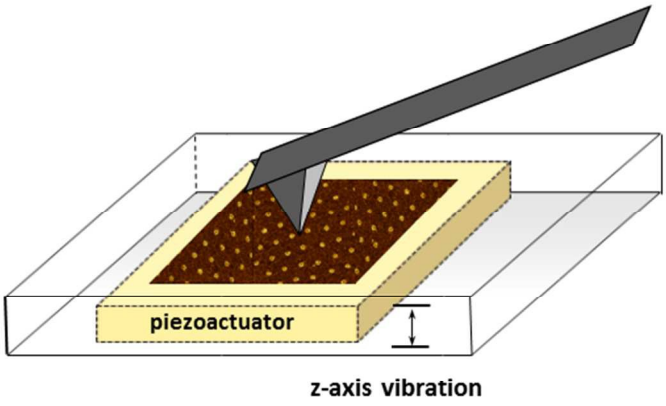

Introduction

Force modulation microscopy (FMM) can be used to identify and map differences in stiffness or elasticity of nanomaterials,[1, 2] to evaluate the composition of materials,[3, 4] and to study variations in crystallinity,[5] polymer phase separation, surface arrangement and distribution.[6-9] Materials that have been studied with FMM include protein-lipid aggregates,[10] patterned self-assembled monolayers (SAMs),[11] wood cells and fibroblasts,[12-14] bacteria,[15] porous silicon,[16] optical thin film materials,[17] as well as polymer blends and resins.[18-21] Molecularly resolved images of polymer crystals have been acquired with FMM.[22, 23] Quantitative measurements can be evaluated using FMM for the Young's modulus and the elasticity of samples. [1, 24-26] With FMM, the intricate details of surface shapes and edges can be revealed with high resolution in ambient conditions to provide a powerful qualitative tool that complements topography imaging.

Since 1991, force modulation microscopy actuation has been achieved by directly driving the z-piezo of the microscope,[1, 7, 19, 27, 28] the bimorph piezoelements of the microscope, [2, 20] by magnetic coatings or particles in an oscillating magnetic field,[3] and by use of external piezoactuators.[17, 29] In this report, force modulation is achieved with an external piezoactuator placed directly underneath the sample. The scanner is operated in contact-mode while the sample is driven to vibrate. The AFM probe is scanned in continuous contact with the surface as the sample is driven to vibrate at selected frequency and amplitude. Information of the topography, elastic response and surface adhesion can be acquired concurrently. The driving frequency,[30] imaging media,[31, 32] tip-sample contact area,[33] amplitude of oscillation,[34] and the shape and stiffness of the tip[9, 35] influence the resolution of FMM amplitude and phase images. A systematic study of the factors which influence the contrast in FMM was previously reported by Jourdan, et al. for nanopatterns inscribed within a film of organosilanes.[31]

With the broad implementation of commercial scanning probe instruments designed to have the tip mounted on the piezotube scanner, it would be practical to develop a sample stage to facilitate sample modulation for FMM experiments. In our studies, a home-built accessory stage for FMM studies was constructed with machined polycarbonate with a piezo actuator element. The operation of the sample stage was evaluated by characterizing three test samples with nanoscale dimensions. Test structures of nanoholes within a film of octadecyltrichlorosiloxane (OTS) provide two distinct surface regions as the simplest platform for FMM studies. Ring-shaped nanostructures prepared on Si(111) with 2-[methoxy (polyethyleneoxy)propyl]trichlorosilane (PEG-silane) provide three domains for evaluating FMM data. Finally, a complex sample consisting of a cyclic gel polymer of poly(N-methyl-glycine)$_{100}$-*b*-poly(N-decyl-glycine)$_{10}$ containing fibrils was selected for FMM studies. Experiments were accomplished in ambient conditions using conventional soft cantilevers.

Experimental

Materials and Reagents. Anhydrous toluene from Sigma-Aldrich (St. Louis, MO) was used as a solvent. Ethanol used for cleaning samples was acquired from Pharmco-AAPER (Boucherville, Quebec). Octadecyltrichlorosilane (OTS) and 2-[methoxy(polyethyleneoxy)propyl]trichlorosilane (PEG-silane) were purchased from Gelest (Morrisville, PA) and used without further purification. Pieces (5 × 7 mm) of polished Si(111) doped with boron (Ted Pella, Inc., Redding, CA) were used as substrates for preparing nanopatterned films. Substrates were cleaned by immersion in piranha solution for 1.5 h. Piranha solution is a mixture of sulfuric acid (Sigma-Aldrich) and hydrogen peroxide (30%, Sigma-Aldrich) at a ratio of 3:1 (v/v). This solution is highly corrosive and should be handled with caution. Silicon substrates were then rinsed copiously with water (Milli-Q, Millipore, Bedford,

MA) and dried with argon. Monodisperse polystyrene (496 ± 8.1 nm) and silica (0.49 ± 0.02 μm) solutions were purchased from Duke Scientific (Palo Alto, CA). The mesospheres were washed with deionized water by centrifugation to remove contaminants such as charge stabilizers or surfactants.

Atomic Force Microscopy. A Keysight model 5500 scanning probe microscope (SPM) equipped with a multipurpose scanner was used for AFM characterizations (Keysight Technologies, Tempe, AZ). The scanner has interchangeable nosecones for selected imaging modes. An empty plastic nosecone assembly (the contact-mode nosecone) without metal components was used for force modulation experiments. Silicon nitride cantilevers with an average force constant of 0.1 N m^{-1} and resonance frequency of 38 kHz were used for FMM imaging (MSCT, Bruker, Camarillo, CA). Picoview v1.12 software was used for data acquisition. Images were processed with Gwyddion (version 2.31) open software supported with Czech Metrology Institute, which is available online.[36]

Results and Discussion

Design of the FMM Sample Stage. The sample stage was made with machined polycarbonate with a shape that was designed for operation with a Keysight 5500 SPM. A photograph of the stage is shown in Fig. 1, indicating the location of the piezoactuator and the Bayonet Neill–Concelman (BNC) cable connection. The essential component of the FMM stage is the piezoactuator element (dimensions: 1 × 1 × 0.2 cm), which enables a z-displacement of 2.2 μm in the range of 0-100 V input and has an axial resonance frequency of 600 kHz (Part number PL088.31, Physik Instrumente, Auburn, MA). This piezoactuator was chosen because of the long operating voltage range, compact size and shape, fast response rate and sub-nanometer resolution. For FMM studies, the voltages applied to the piezoactuator ranged from 0.05-0.5 V.

The black and red wires connect the piezoactuator to the BNC cable which enables input of an AC signal to the stage to induce the vibration of the piezoelement. With the Keysight 5500 instrument, a magnetic mode controller (MAC-mode) was used as an AC source by connecting to the AAC output channel. There are three round flat magnets to attach the sample stage to the scanner housing. Two alignment tracks were machined into the polycarbonate sample holder for translating the sample stage in the x and y direction. A small magnet was embedded within the center of the stage above the piezoactuator to attach samples. Samples for FMM studies can

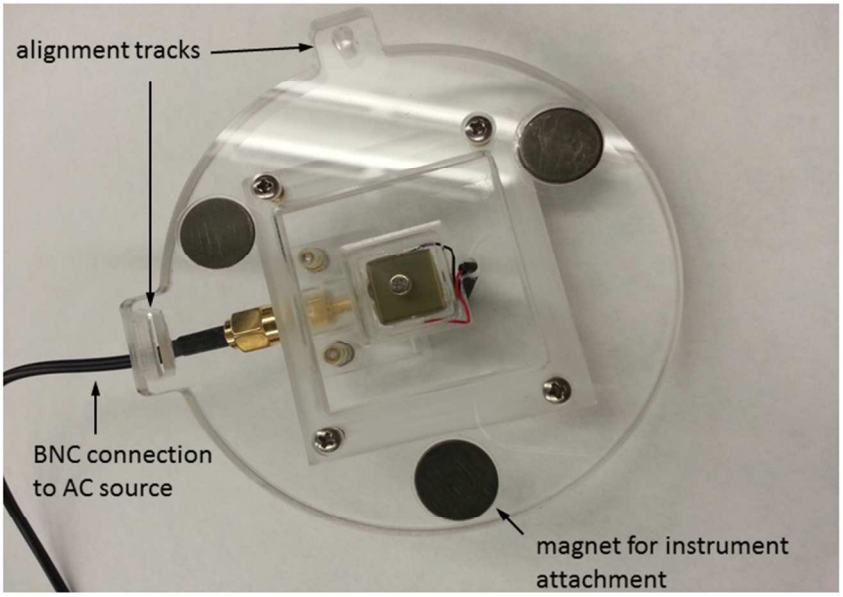

Fig. 1 Photograph of the polycarbonate FMM sample stage. The square piece at the center of the stage is the piezoactuator, with a small circular magnet placed at the center for attaching samples.

either be magnetically clamped, taped or glued to the center of the stage. Further technical details of the physical dimensions of the stage are provided in *Supporting Information*, Fig. S1.

Characterization of Nanopatterns within an OTS Film using the FMM Sample Stage. A test sample of OTS nanopatterns formed on Si(111) was prepared, to evaluate the operation and sensitivity of the FMM sample stage. Details of the procedure for preparing samples using

particle lithography with OTS were previously reported and are presented as *electronic supplementary information*, Fig. S2.[37] Experiments were designed to test the effect of turning the drive on or off as well as evaluating changes in images for selected frequencies. Simultaneously acquired channels for topography, amplitude, and phase are shown side-by-side in Fig. 2 for the

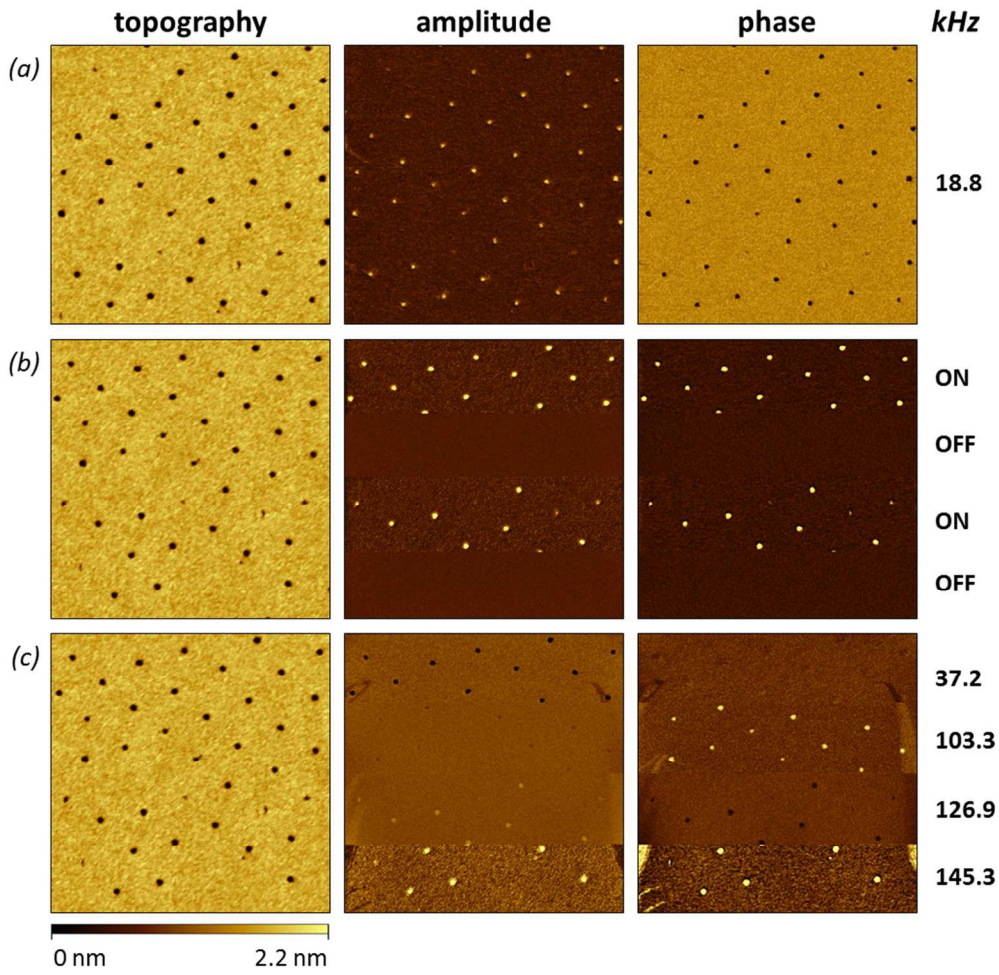

Fig. 2 Sample of nanopores within a thin film of OTS characterized with the FMM sample stage. (a) Images acquired at frequency of 18.8 kHz. (b) Image acquired with the drive turned on or off at a frequency of 145.3 kHz. (c) Dynamic FMM study with ramping of the frequency parameters during a single scan. The size of the images are 3×3 μm^2.

sample of OTS nanopores. The same area was scanned multiple times using selected parameters for sample modulation. A hexagonal arrangement of nanopores is visible in the topography frames, which exhibit reproducible morphologies despite changes in frequency and amplitude

parameters. There are two distinct domains for the nanopatterned sample revealed in the topography frames, the dark spots are areas of uncovered substrate which were protected by silica mesospheres during the OTS immersion step. The brighter areas of the topography frames are the matrix film of OTS. After the mask of mesospheres was removed, a periodic arrangement of nanopores is evident throughout the sample, approximately 3% of the surface is covered with nanoholes. The distance between adjacent nanopores measures 490 ± 44 nm, note that the nanopores are much smaller (110 ± 10 nm diameter, n = 50, the error term is standard deviation) than the size of the 500 nm silica mesospheres used as a surface mask. This is because the area of close contact between the sphere and the substrate is quite small. The depth of the nanopores measured 2.0 ± 0.2 nm.

Changes in the bright or dark contrast of the nanopore areas are reversed for the amplitude versus phase channels in Fig. 2a, when imaging at frequency of 18.8 kHz. The phase images do not necessarily correlate with the stiffness of the samples. The bright or dark regions are highly sensitive to the driving frequency of the sample stage. When the drive is turned off, no features are distinguishable in amplitude and phase images as demonstrated in Fig. 2b. Note that by changing the frequency to 145.3 kHz the hard regions of the substrate have bright contrast in both the amplitude and phase channels. In a dynamic FMM study, the results of selectively ramping the frequency are displayed in Fig. 2c without interruption of data acquisition during a scan. The changes in color contrast for amplitude frames can be interpreted by conducting a frequency sweep experiment, an example spectra is shown in Fig. 3. The areas of the nanopores reveal exposed silicon substrate which is harder compared with the surrounding film of OTS, thus greater amplitude or bright contrast is expected for areas of the nanopores. However, the

results shown in Fig. 2c exhibit a reversal in contrast depending sensitively on the frequency that was selected.

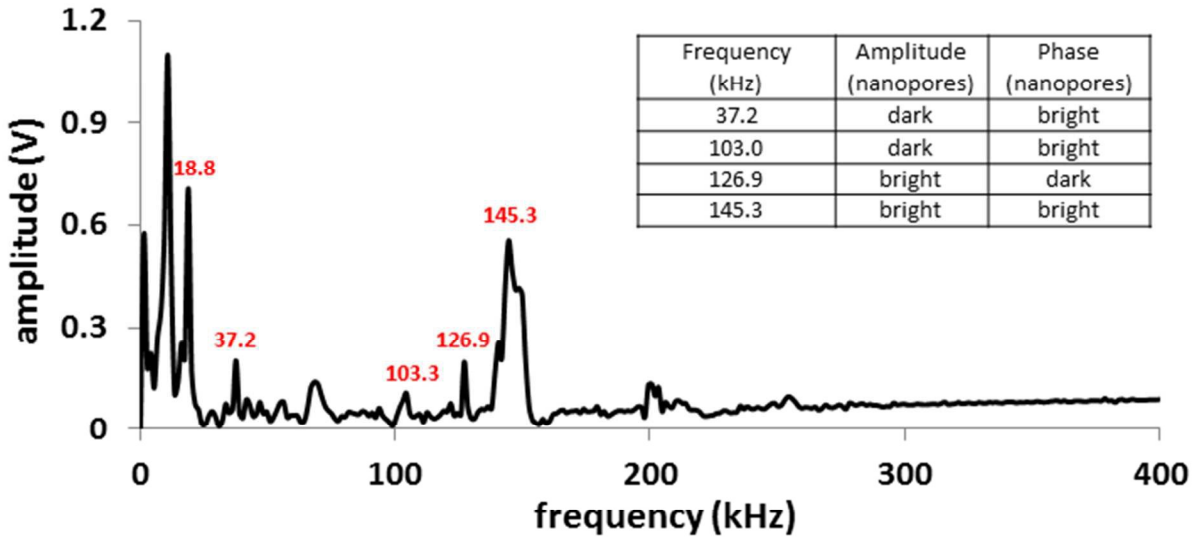

Frequency (kHz)	Amplitude (nanopores)	Phase (nanopores)
37.2	dark	bright
103.0	dark	bright
126.9	bright	dark
145.3	bright	bright

Fig. 3 Frequency sweep experiment with the sample of OTS nanopores.

Clear differences in color contrast between areas of the nanopores and the matrix OTS film are evident in the amplitude and phase images, however using these results to interpret the stiffness of the areas can be complicated. For this example, the larger resonance peaks at 18.8 and 145.3 kHz gave the predicted amplitude response showing bright dots for the locations of the nanopores. The amplitude response of frequency sweeps are excellent predictors of what frequency will tune in amplitude images, however the response for phase images is independent of changes in amplitude.

A further test of the FMM stage was accomplished by zooming-in to view a single nanopore (Fig. 4). At this size scale the irregular outline of a single nanopore becomes apparent. The texture of the OTS film can be resolved, showing a clustered morphology. This example demonstrates the high resolution capabilities that can be achieved with the home-constructed

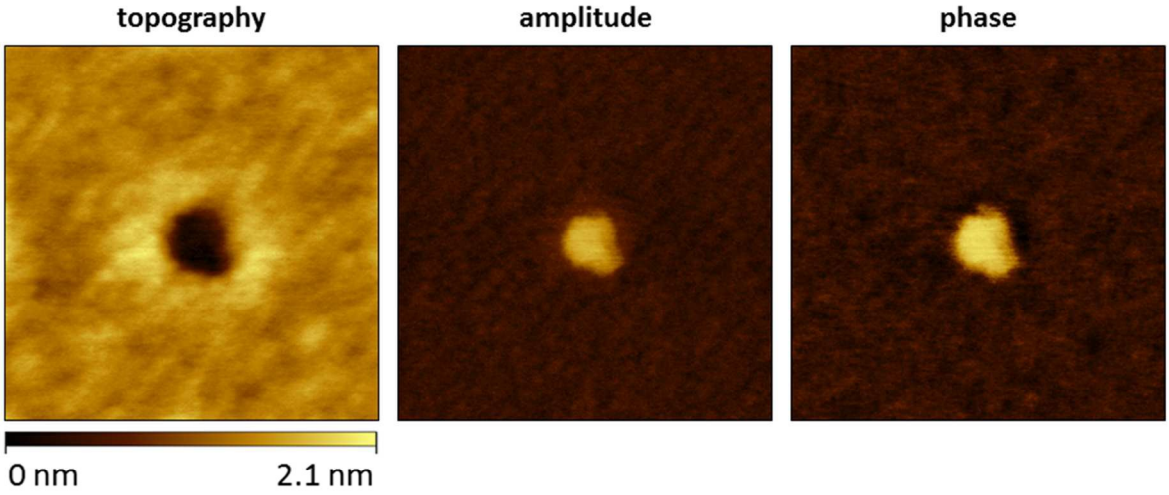

Fig. 4 Details of a single nanopore revealed with FMM. Images were acquired at 145.3 kHz for an area measuring 0.4 × 0.4 μm^2.

FMM sample stage.

Characterization of Nanorings of PEG-silane with FMM

Nanopatterns of PEG-silane rings prepared on Si(111) were characterized with FMM as shown in Fig. 5. For this example, there are three distinct regions visible in the images. There are uncovered areas of the substrate at the centers of the nanorings, the regions of the nanorings are multilayers of PEG-silane, and the areas in between the rings are a relatively homogeneous and compact film of PEG-silane. The sample was prepared using particle lithography combined with heated vapor deposition, as previously described.[38, 39] (Details for sample preparation are also provided in *electronic supplementary information*, Fig. S3.) The areas of the taller nanorings have brighter contrast in the topography images indicating the areas of the multilayer of PEG-

silane, the thickness of the nanorings measures 5.9 ± 1.3 nm. The areas between the nanorings contain a film of PEG-silane. Areas of exposed substrate are located at the very center of the nanorings. The distance between nanorings measured 490 ± 45 nm, which corresponds to the diameter of the latex mesospheres (500 nm) that were used as a surface mask for particle

lithography. The same area was scanned with selected frequencies to evaluate the changes for images shown in amplitude and phase channels (Fig. 5).

Three frequencies (103.3, 150.4, and 187.3 kHz) were selected for Fig. 5 to study the changes for PEG-silane nanorings with FMM. We would predict that areas of the nanorings with

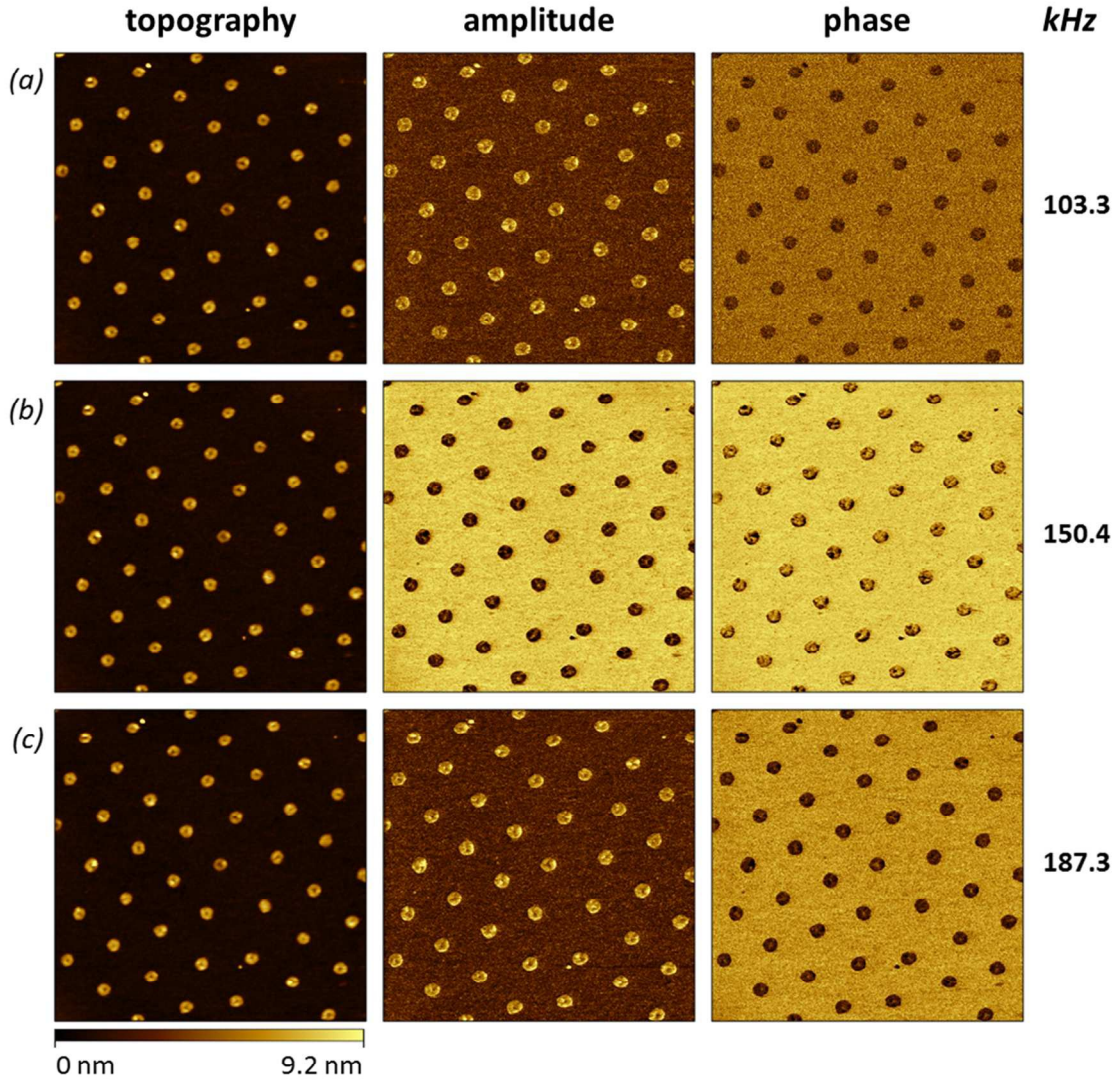

Fig. 5 Images of PEG-silane nanorings acquired with the FMM sample stage at driving frequencies of (a) 103.3 kHz, (b) 150.4 kHz and (c) 187.3 kHz. Images are 3 × 3 μm^2 scan sizes.

a multilayer film of PEG-silane would have the darkest color for the amplitude frames, shown in the center amplitude image acquired at a driving frequency of 150.4 kHz. The nanoring structure is made of multilayers of PEG-silane which is a softer material compared with the surrounding matrix areas and the center of the rings, which leads to a smaller amplitude for the tip indentation. The center amplitude image acquired at 150.4 kHz also sensitively reveals a tiny bright spot at the center of each nanoring for the region of exposed substrate. The images in Figs. 5a and 5c disclose brighter contrast for the PEG-silane nanorings, which does not follow our prediction. Examples of contrast reversal have been previously reported for nanopatterns within an organosilane film.[31] The contrast observed for amplitude and phase images depends sensitively on the modulation parameters of frequency and amplitude as well as the natural resonance of the cantilever.

The frequency spectra acquired for the sample is presented in Fig. 6, which shows the highest amplitude response of the selected frequencies occurs at 150.4 kHz. As with the example of Fig. 2, the optimal frequency for FMM imaging is found at the resonance peaks with higher amplitude response. Brighter contrast for the nanorings was observed for the amplitude channel in Figs. 5a and 5c, suggesting that the selected frequencies of 103.3 and 187.3 kHz were not optimal parameters for resolving differences in elasticity. In these examples, the edge effects and surface adhesion predominate tip-sample interactions rather than differences in stiffness. In the phase channels for all three frequencies viewed in Fig. 6, dark rings and lighter background can be clearly resolved to indicate the relative differences in elastic response between the nanorings and surrounding matrix film of PEG-silane.

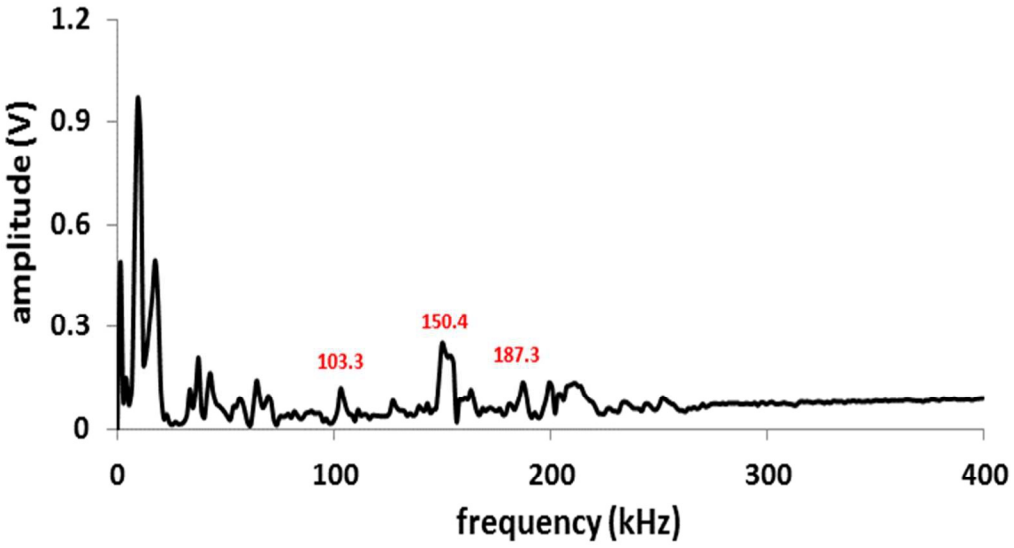

Fig. 6 Frequency sweep acquired with FMM for the sample of PEG-silane nanorings.

Characterization of a Cyclic Gel Sample with FMM. A block copolymer poly(*N*-methyl-glycine)$_{100}$-*b*-poly(*N*-decyl-glycine)$_{10}$, or *c*-PNMG$_{100}$-*b*-PNDG$_{10}$ can form free-standing gels at 5-10 wt% in methanol at room temperature.[40] The gel system contains entangled fibrillar structures that are difficult to resolve with conventional topography images. Fibrils can be faintly resolved in topographs when saturating the color scale during image processing. Synthesis and characterization of the cyclic gel sample was previously reported using tapping-mode AFM.[40] The gel sample is more complex than the previous examples of nanopatterns, it contains both large aggregates and small-embedded fibrils in the gel system. The polymer sample was dissolved in methanol at 1% wt and formed a flow gel after 30 min. A drop of the flow gel (10 μL) was deposited on a piece of freshly cleaved mica(0001), then dried in air before imaging with FMM. Topography, amplitude and phase channels obtained with FMM at four selected frequencies are shown in Fig. 7. The same area of the sample was scanned (8 × 8 μm^2) with changes of the frequency parameters. For the topography frames the details of the small

microfibrils within sample cannot be clearly resolved, however the phase and amplitude images resolve the fine details of the fibril shapes and locations.

The fibrils are stiffer materials compared with the surrounding gels, therefore larger

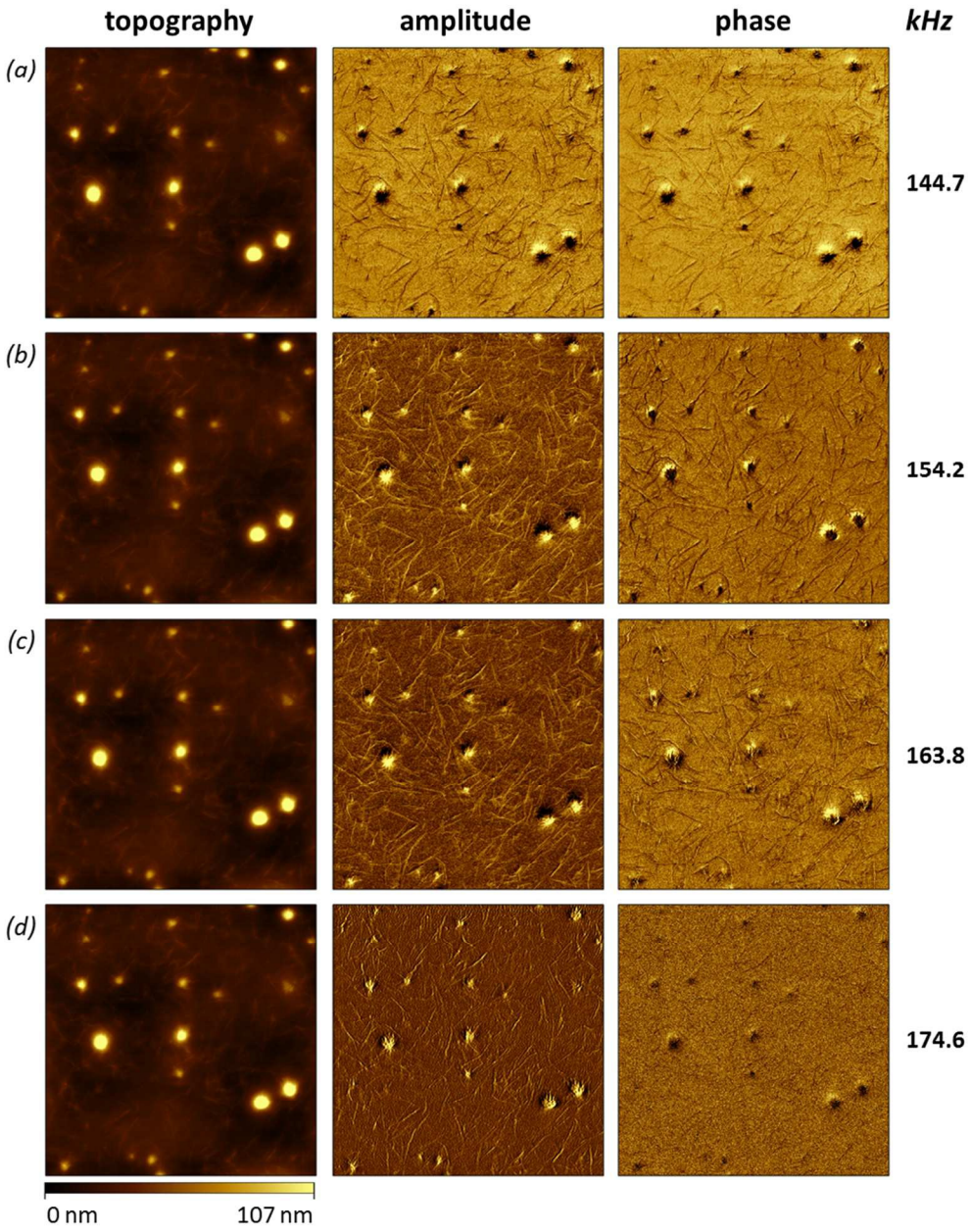

Fig. 7 Images of the cyclic gel sample obtained with FMM at driving frequencies of (a) 144.7, (b) 154.2, (c) 163.8, (d) 174.6 kHz. The frames are $8 \times 8\ \mu m^2$ scans.

amplitude or bright contrast is expected for the fibrils as revealed in the amplitude frames of Figs. 7b-7d. Contrast reversal is shown in Fig. 7a, where the fibrils are darker in color for the amplitude frame. The phase images have excellent resolution for the phase frames acquired at frequencies of 144.7, 154.2, and 163.8 kHz, disclosing exquisite details of the fibril morphology (Figs. 7a-7c). However at a frequency of 174.6 kHz (Fig. 7d) the locations of the fibrils are not distinguishable in the phase image. The results suggest that the optimized parameters for FMM experiments selected for the amplitude channel are not necessarily the same frequency for optimizing the phase images.

The frequency sweep when imaging the cyclic gel sample is shown in Fig. 8. The lowest resolution found at frequency of 174.6 kHz correlates with the smallest amplitude response. At this frequency the vibration amplitude is not sufficient to fully reveal differences in elastic response. However, for the other three frequencies tested with FMM, sufficient energy is supplied to acquire high resolution images for both phase and amplitude channels.

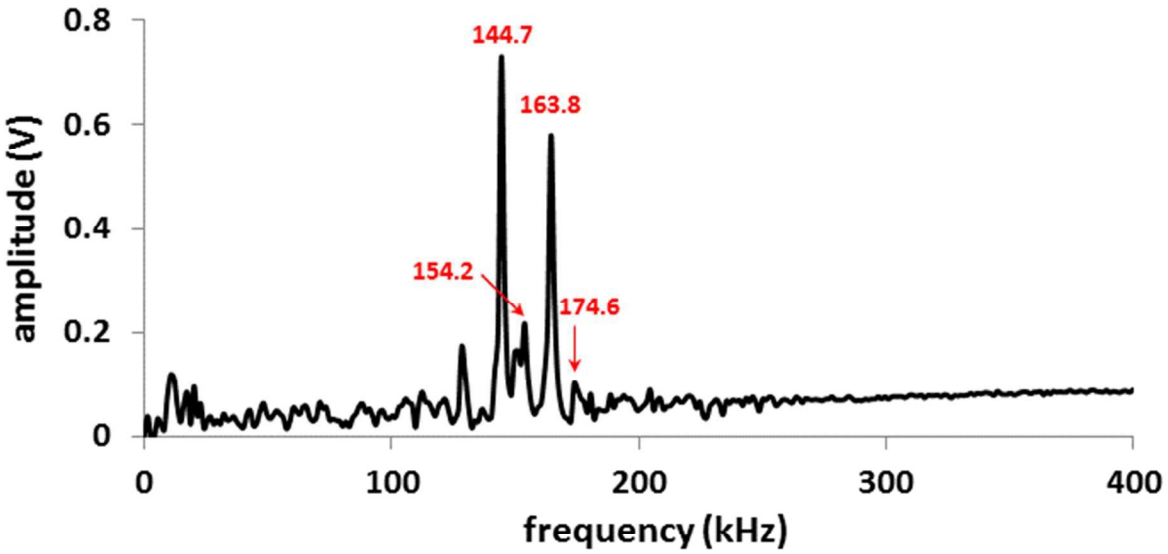

Fig. 8 Frequency spectrum acquired with the FMM sample stage for the cyclic gel sample (*c*-PNMG$_{100}$-*b*-PNDG$_{10}$).

Driving frequencies were selected to avoid external resonances outside the system. An example of a frequency sweep before and after the tip is engaged with sample is shown in Fig. S4 in *electronic supplementary information*. When the AFM tip is not in contact with the sample, only a few resonance peaks are detected in the frequency sweep, indicating resonances from the instrument set-up. When the tip is contact with sample, more peaks appear indicating the resonances from tip-sample contact.

Both the driving frequency and the amplitude of the resonance peak determine the resolution of the FMM amplitude and phase channels. Weaker resonance peaks were shown to display a contrast reversal for elastic response. For the sample of OTS nanopores and the nanorings of PEG-silane, stronger resonance peaks were found at frequencies below 25 kHz. The voltages applied to the piezoactuator of the stage were 0.4 V for the OTS nanopores and 0.5 V for PEG-silane nanorings. For the nanopatterned surfaces of OTS and PEG-silane the overall z scale measured less than 10 nm (*electronic supplementary information*, Fig. S5), while the cyclic gel sample had taller features of 160 nm (*electronic supplementary information*, Fig. S6). For the complicated system of the cyclic gel sample, which has larger aggregates along with micron-sized fibrils embedded in the gel system, stronger resonance peaks were detected in the frequency range of 120-180 kHz using 0.05 V applied to the piezoactuator.

Conclusions

Excellent resolution can be achieved when using a home-constructed FMM sample stage designed with a tip-mounted scanner, even for complex surfaces or multi-component samples. The prototype FMM stage is suitable for experiments with samples in ambient conditions and exhibited high resolution when parameters were optimized. Our system is not intended so much for advanced quantitative experiments, it provides a tool to enable basic qualitative comparisons

of the elastic response of samples as well as for mapping structural domains. Interpretation of FMM amplitude frames can be complicated for acquiring quantitative measurements of elastic response, in which the parameters for driving frequency and amplitude require optimization. Knowledge of the sample composition is critical for correctly interpreting information from amplitude and phase images. Future studies will incorporate a liquid cell for the stage design to enable FMM characterizations in liquids. Machined glass components will be used for constructing the sample stage to enable studies in solvents.

ASSOCIATED CONTENT

Electronic Supplementary Information

Additional information (Figs. S1-S6) as described in the text. The Supporting Information is available free of charge on the Publications website.

Acknowledgements

The authors gratefully acknowledge financial support from the National Science Foundation Career/PECASE award (CHE-0847291) and the American Chemical Society Petroleum Research Fund (New Directions Program, 52305-ND). The authors thank Chang-Uk Lee for synthesis of the polymeric gel sample.

References

1. S. O. Akari, E. W. Vandervegte, P. C. M. Grim, G. F. Belder, V. Koutsos, G. Tenbrinke and G. Hadziioannou, *Appl. Phys. Lett.*, 1994, **65**, 1915-1917.
2. B. D. Beake, G. J. Leggett and P. H. Shipway, *Surf. Interface Anal.*, 1999, **27**, 1084-1091.
3. S. Yamamoto and H. Yamada, *Langmuir*, 1997, **13**, 4861-4864.
4. N. Jalili and K. Laxminarayana, *Mechatronics*, 2004, **14**, 907-945.
5. S. N. Magonov and D. H. Reneker, *Annu. Rev. Mater. Sci.*, 1997, **27**, 175-222.
6. R. M. Overney, E. Meyer, J. Frommer, H. J. Guntherodt, M. Fujihira, H. Takano and Y. Gotoh, *Langmuir*, 1994, **10**, 1281-1286.
7. T. Kajiyama, K. Tanaka, I. Ohki, S. R. Ge, J. S. Yoon and A. Takahara, *Macromolecules*, 1994, **27**, 7932-7934.
8. M. Menke, S. Kunneke and A. Janshoff, *Eur. Biophys. J. Biophys. Lett.*, 2002, **31**, 317-322.
9. H. N. Lin, T. T. Hung, E. C. Chang and S. A. Chen, *Appl. Phys. Lett.*, 1999, **74**, 2785-2787.
10. S. Krol, M. Ross, M. Sieber, S. Kunneke, H. J. Galla and A. Janshoff, *Biophys. J.*, 2000, **79**, 904-918.
11. J. L. Wilbur, H. A. Biebuyck, J. C. Macdonald and G. M. Whitesides, *Langmuir*, 1995, **11**, 825-831.
12. B. Clair, R. Arinero, G. Leveque, M. Ramonda and B. Thibaut, *Iawa J.*, 2003, **24**, 223-230.
13. H. Haga, M. Nagayama and K. Kawabata, *Curr. Nanosci.*, 2007, **3**, 97-103.
14. S. Sasaki, M. Morimoto, H. Haga, K. Kawabata, E. Ito, T. Ushiki, K. Abe and T. Sambongi, *Arch. of Histol. Cytol.*, 1998, **61**, 57-63.
15. M. Fritz, M. Radmacher, N. Petersen and H. E. Gaub, *J. Vac. Sci. Technol. B*, 1994, **12**, 1526-1529.
16. F. Sbrana, M. Ghulinyan and L. Pavesi, *Phys. Status Solidi A* 2005, **202**, 1492-1496.
17. N. Sahoo, S. Thakur, M. Senthilkumar and N. C. Das, *Appl. Surf. Sci.*, 2003, **206**, 271-293.
18. B. Nysten, R. Legras and J. L. Costa, *J. Appl. Phys.*, 1995, **78**, 5953-5958.
19. H. Y. Nie, M. Motomatsu, W. Mizutani and H. Tokumoto, *J. Vac. Sci. Technol. B*, 1995, **13**, 1163-1166.
20. A. A. Galuska, R. R. Poulter and K. O. McElrath, *Surf. Interface Anal.*, 1997, **25**, 418-429.
21. I. S. Gilmore, M. P. Seah and J. E. Johnstone, *Surf. Interface Anal.*, 2003, **35**, 888-896.
22. K. Kimura, K. Kobayashi, H. Yamada and K. Matsushige, *Nanotechnology*, 2007, **18**.
23. K. Kimura, K. Kobayashi, H. Yamada and K. Matsushige, *Nanotechnology*, 2008, **19**.
24. D. DeVecchio and B. Bhushan, *Rev. Sci. Instrum.*, 1997, **68**, 4498-4505.
25. M. Troyon, Z. Wang, D. Pastre, H. N. Lei and A. Hazotte, *Nanotechnology*, 1997, **8**, 163-171.
26. O. Pietrement and M. Troyon, *Tribol. Lett.*, 2000, **9**, 77-87.
27. M. Radmacher, R. W. Tilmann and H. E. Gaub, *Biophys. J.*, 1993, **64**, 735-742.
28. R. M. Overney, H. Takano and M. Fujihira, *Europhys. Lett.*, 1994, **26**, 443-447.
29. H. U. Krotil, T. Stifter and O. Marti, *Rev. Sci. Instrum.*, 2000, **71**, 2765-2771.
30. W. Kiridena, V. Jain, P. K. Kuo and G. Y. Liu, *Surf. Interface Anal.*, 1997, **25**, 383-389.

31. J. S. Jourdan, S. J. Cruchon-Dupeyrat, Y. Huan, P. K. Kuo and G. Y. Liu, *Langmuir*, 1999, **15**, 6495-6504.
32. W. J. Price, P. K. Kuo, T. R. Lee, R. Colorado, Z. C. Ying and G. Y. Liu, *Langmuir*, 2005, **21**, 8422-8428.
33. G. Bar, S. Rubin, A. N. Parikh, B. I. Swanson, T. A. Zawodzinski and M. H. Whangbo, *Langmuir*, 1997, **13**, 373-377.
34. J. S. G. Ling and G. J. Leggett, *Polymer*, 1997, **38**, 2617-2625.
35. R. Resch, G. Friedbacher, M. Grasserbauer, T. Kanniainen, S. Lindroos, M. Leskela and L. Niinisto, *Appl. Surf. Sci.*, 1997, **120**, 51-57.
36. D. Nečas and P. Klapetek, *Cent. Eur. J. Phys.*, 2012, **10**, 181-188.
37. M. Overney René and V. Tsukruk Vladimir, in *Scanning Probe Microscopy of Polymers*, American Chemical Society, ACS Symposium Series, 1998, vol. 694, ch. 1, pp. 2-30.
38. E. L. Florin, M. Radmacher, B. Fleck and H. E. Gaub, *Rev. Sci. Instrum.*, 1994, **65**, 639-643.
39. P.-E. Mazeran and J.-L. Loubet, *Tribol. Lett.*, 1997, **3**, 125-132.
40. C.-U. Lee, L. Lu, J. Chen, J. C. Garno and D. Zhang, *ACS Macro Lett.*, 2013, **2**, 436-440.